Zero Common-Mode Voltage Modulation for Flying-Capacitor-Based Vienna Rectifier With Consideration of Nonideal Factors

Hui Liu, *Student Member, IEEE*, Dong Jiang, *Senior Member, IEEE*, Shuyu Zhang, Xuan Zhao, *Student Member, IEEE*, and Zicheng Liu, *Member, IEEE*

***Abstract*—This article analyzes the common-mode voltage (CMV) of the Vienna rectifier and proposes a CMV elimination strategy. The proposed method reduces the neutral-point voltage (NPV) fluctuation by introducing an auxiliary flying capacitor (FC) leg and suppresses low-frequency fluctuations of CMV through zero CMV (ZCMV) modulation. Aimed at the high-frequency spikes of CMV, an analysis of nonideal factors, including unidirectional conduction of the diode, current distortion, and current ripple and control delay is conducted leading to the proposal of a novel compensation method called FC-ZCMV-C. Experimental results indicate that, without affecting the power factor of the rectifier, FC-ZCMV-C further suppresses the CMV spikes, significantly reducing common-mode electromagnetic interference by 10–20 dB.**

***Index Terms*—Compensation for nonideal factors, current distortion, flying capacitor (FC) leg, Vienna rectifier, zero common-mode voltage (CMV).**

I. Introduction

With the continuous optimization of power switching devices and computer technology, the field of power electronics has witnessed significant advancements. Simultaneously, the operation of numerous power electronic devices has introduced a substantial amount of harmonic pollution to the power grid. Vienna rectifier is a three-level topology that has the advantages of high power density, high power factor, and good current harmonic characteristics, switches only need to withstand half the voltage and do not need to consider the dead zone [1]. As a result, it has become a major focus in the current realm of power electronics. Consequently, it finds widespread applications in fields such as electric vehicle charging [2], power factor correction [3], and renewable energy generation [4].

Frequent switching of the power devices inevitably leads to higher dv/dt and di/dt, thereby generating electromagnetic interference (EMI). EMI will be spread by conduction or radiation. Based on different propagation paths, conducted EMI can be divided into common-mode (CM) interference and differential-mode interference [6]. The CM EMI is generated by the common-mode voltage (CMV) in the coupling loop formed by the rectifier and the ground, in the form of CM current. In motor control systems, bearing currents can reduce the lifespan of bearings [7]. In photovoltaic systems, CM leakage currents can damage photovoltaic panels [8]. Additionally, CMV can also emit CM EMI, thereby posing a threat to the safe and reliable operation of other systems located in the vicinity of the rectifier.

The use of filters can reduce the CM EMI of rectifiers [9]. However, the introduction of passive components adds to the system's size and weight [10]. Active EMI filters, employing sampling compensation, can reduce CM EMI while also decreasing the volume of passive components. Nevertheless, they introduce additional control boards, increasing system complexity [11]. Although various methods can alleviate issues caused by CMV, these methods bring more electronic devices and complexity to the system. Therefore, another straightforward and cost-effective solution is based on pulse width modulation (PWM)-driven active suppression techniques, which suppress CMV at its source, reducing the reliance on EMI filters and enhancing system power density.

In three-phase systems, CMV can be represented by the average value of the three-phase ac side voltage. A modulation strategy based on hybrid voltage vector preselection was proposed by avoiding the use of two zero vectors in the two-level inverter [12]. This approach significantly reduces the peak of the CMV in the seventh sector of the current, and also notably decreases the total harmonic distortion (THD) and ripple of the current. Un and Hava [13] avoided the occurrence of a CMV with an amplitude of $V_{dc}/2$ by synthesizing the reference voltage using adjacent three nonzero vectors. In addition, due to discontinuous modulation, the method benefits from reduced switching losses. However, this method is only suitable for operation at a modulation index value larger than 0.61. To restrain the CMV for back-to-back two-level converters, a CMV reduction method based on zero-sequence voltage injection is proposed in [14]. By injecting the optimal amount of zero-sequence voltage on either the rectifier-side or the inverter-side, the corresponding pulse overlapping areas that result in high CMV amplitudes can be eliminated with the proposed method, then the amplitude of CMV can be reduced by half, and the pulse edges of CMV can be reduced by one-third. However, these methods can only

Manuscript received 21 March 2024; revised 5 June 2024; accepted 22 June 2024. Date of publication 29 July 2024; date of current version 24 December 2024. *(Corresponding author: Xuan Zhao.)*

The authors are with Huazhong University of Science and Technology, Wuhan Hubei 430074, China (e-mail: liuhuihui@hust.edu.cn; jiangd@hust.edu.cn; mojisama0@gmail.com; zhaoxuan95@hust.edu.cn).

Digital Object Identifier 10.1109/TIE.2024.3423368

0278-0046 © 2024 IEEE. Personal use is permitted, but republication/redistribution requires IEEE permission.
See https://www.ieee.org/publications/rights/index.html for more information.

Authorized licensed use limited to: Univ of Calif Berkeley. Downloaded on October 27,2026 at 23:27:44 UTC from IEEE Xplore. Restrictions apply.

reduce the amplitude of CMV to $V_{dc}/6$. Since the ac side voltage of a three-phase, two-level converter can only be $\pm V_{dc}/2$ per phase, the CMV obtained by summing the three phases can never reach zero. To achieve zero CMV (ZCMV), the introduction of new degrees of freedom is necessary, such as additional voltage levels or novel connection configurations. Chen et al. Chen et al. [15] derived the expression for the CMV of the modular multilevel converter. By ensuring that the number of on-state submodules in the upper bridge arm equals the number in the lower bridge arm, selecting the nearest voltage vector for modulation achieved effective suppression of CMV. The positive and negative pulses of the rectifier and inverter side phase voltages in a carrier period are rearranged and the CMV in back-to-back three-level neutral point clamped (NPC) in [16] is eliminated by aligning the edges of the positive voltage pulses with the edges of the negative voltage pulses in the phase voltage group. A new H10 inverter topology for two-level, three-phase inverter applications was proposed in [17]. The proposed topology can achieve constant CMV or ZCMV. But it will increase the number of switches. Shen et al. [18] eliminated the overall CM interference in the asymmetrical six-phase permanent magnet synchronous motor by causing two sets of two-level inverters to generate completely opposite CMV. By employing the method of virtual space vector PWM and relinquishing the use of certain voltage vectors, [19] reduced the CMV of the three-level NPC inverter from $V_{dc}/3$ to $V_{dc}/6$. Additionally, by adjusting the variable coefficient of the virtual vector, it acquired the capability to control the midpoint voltage across the full modulation index. However, the CMV still remains relatively high. Moreover, the neutral-point voltage (NPV) fluctuation can result in low-frequency fluctuation in CMV. While suppressing CMV, maintaining a balanced control of the NPV has become a new challenge. Due to the unidirectional conductivity of diodes, distortion occurs when the current of the Vienna rectifier crosses zero. Furthermore, there is inevitably communication delay between the PWM signals and the final output signals in the actual system [20]. ZCMV modulation typically requires edge cancellation of pulses from different bridge arms, necessitating precise control of the edge synchronization of power pulses. However, due to pulse delays, ZCMV can only achieve synchronization of digital pulses and cannot ensure synchronization of power pulses. As a result, high-frequency spikes persist within the CMV. Addressing nonideal factors, a method utilizing disturbance observers to compensate for inverter voltage distortion was proposed in [21]. Miao et al. [22] analyzed two cases of current distortion in the Vienna rectifier, then the equivalent *dq*-frame zero-crossing effect model is proposed. Finally, methods for compensating current distortion are provided. But it did not consider the suppression of CMV. Xing et al. [23] introduced a two-level PWM scheme based on vector selection. In the first layer, the fluctuation of NPV and the amplitude of CMV are reduced by choosing specific voltage vectors. In the second layer, current distortion is reduced by reselecting switch states. However, this method still results in a CMV amplitude of $V_{dc}/6$. In [24], we proposed a method to achieve ZCMV in the Vienna rectifier while simultaneously reducing the fluctuation of NPV by adding an external flying capacitor (FC) leg. However, we found that even with the use of ZCMV, there are still significant spikes of CMV near the current crossing zero. Therefore, this article starts with the topology of the Vienna rectifier and takes into account the impact of various nonideal factors. Then a method to completely eliminate the CMV is proposed, which can significantly reduce the harm of CM EMI.

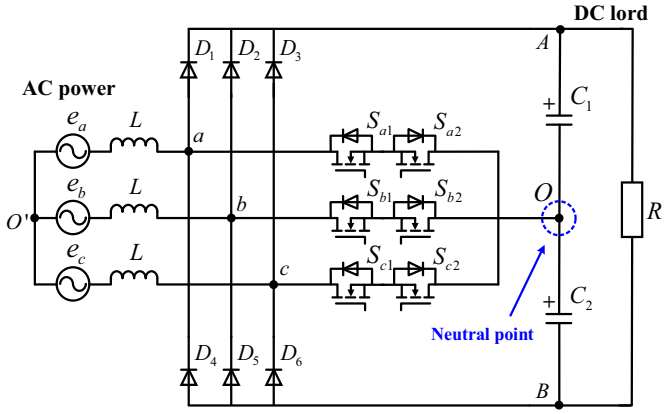


Fig. 1. Circuit of Vienna rectifier.

Section II presents the fundamental principles of the Vienna rectifier and ZCMV modulation. Then, the impact of NPV on ZCMV is deduced. Section III focuses on using FC-leg to suppress the NPV fluctuation, thereby reducing the threefold fundamental frequency fluctuation in CMV while improving power quality and reducing EMI. Section IV analyzes the impact of diode unidirectional conductivity, phase differences between current and voltage, current distortion, current ripple and communication delays on CMV elimination. Then, a compensation method for ZCMV considering various nonideal factors is proposed, theoretically ensuring CMV remains zero. Section V validates the approach within the Matlab/Simulink model. Section VI establishes an experimental platform for verification. Section VII provides a summary of this article. The modulation method proposed in this article can effectively suppress CMV without affecting power factor, resulting in a reduction of conducted EMI by 10–20 dB. At the same time, it can significantly reduce the fluctuation of NPV, and it can also suppress current distortion. The FC-leg adds very little to the cost and does not increase the size of the system. The disadvantage is that the THD of the current is increased and the modulation index is reduced.

II. ZCMV of Vienna Rectifier

A. Basic Principle of Vienna Rectifier

The topology of the Vienna rectifier is shown in Fig. 1, where e_a, e_b, and e_c are the grid voltage, i_a, i_b, and i_c are the ac current, u_a, u_b, and u_c are the input voltage of the rectifier. L is the ac side filtering inductance, R_s is the equivalent resistance. D_1–D_6 are diodes, S_{a1}–S_{c2} are switches, C_1 and C_2 are dc side voltage dividing capacitors, R is the load. A and B are the positive and negative poles of the dc side, O is the dc side neutral point, and O' is the ac side midpoint.

Authorized licensed use limited to: Univ of Calif Berkeley. Downloaded on October 27,2026 at 23:27:44 UTC from IEEE Xplore. Restrictions apply.

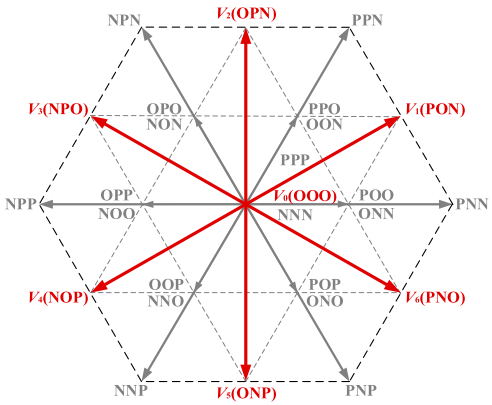


Fig. 2. Space vector diagram of Vienna.

TABLE I
VECTOR AND CMV OF THE VIENNA

Vector	|CMV|
PPP, NNN	$V_{dc}/2$
PPO, OPP, POP, ONN, NON, NNO	$V_{dc}/3$
PPN, NPP, PNP, POO, OPO, OOP, PNN, NPN, NNP, OON, NOO, ONO	$V_{dc}/6$
OOO, PON, OPN, NPO, NOP, ONP, PNO	0

Taking O as the voltage reference point, three output states S_x ($x = a, b, c$) are defined for each phase. Taking phase a as an example, when both switches S_{a1} and S_{a2} are turned on, point a is connected to point O, and at this moment, $u_a = 0$, $S_x = \mathrm{O}$. When both switches for phase a are turned off, if the current flows from the ac side into point a, then point a is connected to point A through diode D_1, and $u_a = V_{dc}/2$, $S_x = \mathrm{P}$. If the current flows out of point a into the ac side, then point a is connected to point B through diode D_4, and $u_a = -V_{dc}/2$, $S_x = \mathrm{N}$. Therefore, each phase of the Vienna rectifier can output three voltage levels, and the voltage is jointly determined by the status of the switch and the direction of the current.

Taking phase a as an example, according to Kirchhoff's voltage law (KVL), we can get

$$e_a + L\frac{di_a}{dt} + R_s i_a + u_a = u_{O'O}. \tag{1}$$

B. ZCMV Modulation

The CMV of the Vienna rectifier can be expressed as the average of the ac voltage of the three phases

$$u_{\mathrm{CMV}} = \frac{1}{3}(u_a + u_b + u_c). \tag{2}$$

Voltage vectors are defined based on the state of each phase of the Vienna rectifier. For instance, the vector "PON" represents $u_a = V_{dc}/2$, $u_b = 0$, and $u_c = -V_{dc}/2$. As shown in Fig. 2, excluding unused combinations PPP and NNN, the vectors can be categorized into four groups based on their length: one zero vector, 12 small vectors, six medium vectors, and six large vectors. By using the equation of CMV (2), the magnitude of CMV for the voltage vectors can be determined as shown in Table I.

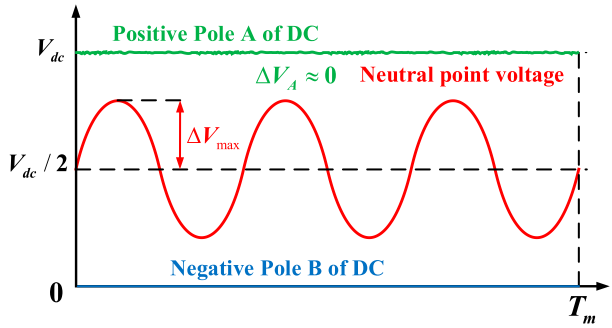


Fig. 3. Voltages at points A, B, and O.

SVPWM, due to the usage of small vectors, results in a CMV of $\pm V_{dc}/3$. If only large vectors, medium vectors, and zero vectors are used for modulation, the CMV will become $\pm V_{dc}/6$. In this article, only medium vectors and zero vectors are used, so the CMV is 0.

Compared with SVPWM, ZCMV increases the distance of vector synthesis and therefore increases the THD of the current. At the same time, the modulation index is reduced to 0.866, which is a defect in most of ZCMVs [25], [26], [27]. Han et al. [28] added a phase bridge arm to the three-phase, two-level inverter to realize ZCMV, and its modulation index is 1. However, this method requires the addition of an extra set of L-C filters. The purpose of the FC-leg proposed in this article is to reduce the fluctuation of NPV. Therefore, such as most ZCMVs, the modulation index is also 0.866.

C. The Impact of NPV on ZCMV

In this section, the negative pole B of the dc side in Fig. 1 is taken as the reference potential ($V_B = 0$), and the voltage at the positive pole A on the dc side is $V_A = V_{dc} + \Delta V_A$. Due to the employment of closed-loop control, ΔV_A is approximately zero. The voltage at the neutral point O is $V_{\mathrm{NPV}} = V_{dc}/2 + \Delta V$. Fig. 3 illustrates the voltage waveforms at three points, where $\Delta V_{\max}$ is the magnitude of NPV fluctuations.

When the zero vector [OOO] is applied, the voltages on the ac side of the three phases are all V_{NPV}. When the middle vectors [PON, OPN, NPO, NOP, ONP, and PNO] are applied, one phase is V_A, one phase is V_B, and one phase is V_{NPV}. Therefore, as shown in the following equations, even when using ZCMV, there still exists a fluctuating component of NPV in CMV. Since ZCMV cannot control NPV, the peak value of CMV remains high at certain instants, as shown in Fig. 4:

$$[\mathrm{OOO}]: u_{\mathrm{CMV}} = \frac{1}{3}(u_a + u_b + u_c) = \frac{1}{2}V_{dc} + \Delta V \tag{3}$$

$$[\mathrm{NOP}]: u_{\mathrm{CMV}} = \frac{1}{3}(u_a + u_b + u_c) = \frac{1}{2}V_{dc} + \frac{1}{3}\Delta V. \tag{4}$$

III. FC-VIENNA

Using only medium and zero vectors for modulation can lead to excessive NPV fluctuation, thereby affecting the quality of

Authorized licensed use limited to: Univ of Calif Berkeley. Downloaded on October 27,2026 at 23:27:44 UTC from IEEE Xplore. Restrictions apply.

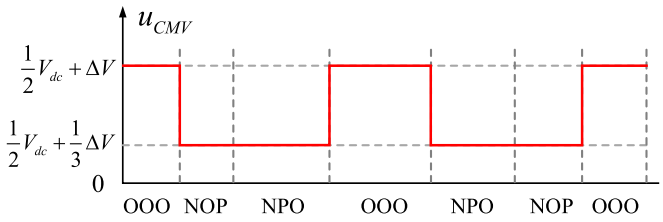


Fig. 4. CMV generated by NPV (in one switching cycle of ZCMV).

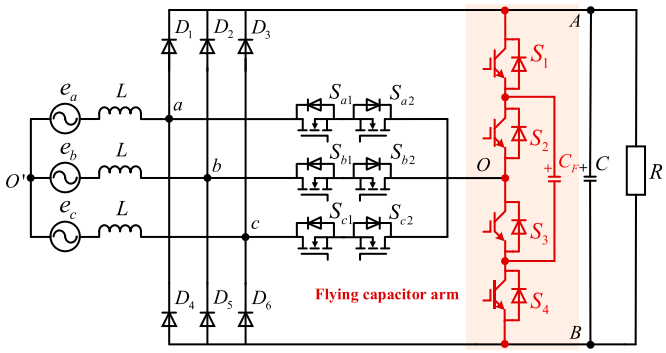


Fig. 5. FC-Vienna.

the output electrical energy, and it also increases EMI. To suppress the NPV fluctuation, a Vienna topology with a FC-leg, as shown in Fig. 5, was designed.

The FC leg consists of four switches (S_1–S_4) and a capacitor (C_F). The positive direction of current flow is from the neutral point to the three-phase bridge arm, as depicted in Fig. 6. Here, the current flows from the neutral point to the three-phase bridge arm in a positive direction. When $i_{\text{mid}} > 0$, when the switch state [S_1, S_2, S_3, S_4] is 0101, the capacitor discharges and the voltage of the capacitor decreases; when the switch state is 1010, the capacitor charges and the voltage of the capacitor increases. When $i_{\text{mid}} < 0$, when the switch state is 0101, the capacitor is charged and the voltage of the capacitor increases; when the switch state is 1010, the capacitor is discharged and the voltage of the capacitor decreases.

The control of the FC-leg and the Vienna rectifier is completely decoupled, as shown in Fig. 7. Here, $0.5V_{\text{dc}}$ is half of the dc-side voltage, v_{FC} is the voltage of the capacitor of the FC-leg, i_{mid} is the midpoint current, and it is considered positive in the direction shown in Fig. 6(a). The fixed duty cycle of 0.5 signifies that the times for 0101 and 1010 are completely synchronized, resulting in a nearly identical charging and discharging effect on the capacitor. Δd is the duty cycle correction for controlling the NPV and is calculated using the following equation:

$$\Delta d = (0.5V_{\text{dc}} - v_{\text{FC}})\left(K_P + \frac{K_I}{s}\right)\text{sign}(i_{\text{mid}}) \tag{5}$$

where K_P and K_I are the coefficients of the PI controller, and sign(x) is the sign function. When $x \geq 0$, sign(x) = 1. When $x <$ 0, sign(x) = –1. The duty cycle for FC-leg's S_1 and S_3 is d^*($d^* = 0.5 + \Delta d$). PWM are generated by comparing them

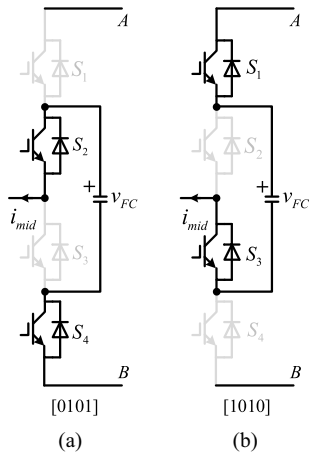


Fig. 6. Status of the FC leg. (a) [0101]. (b) [1010].

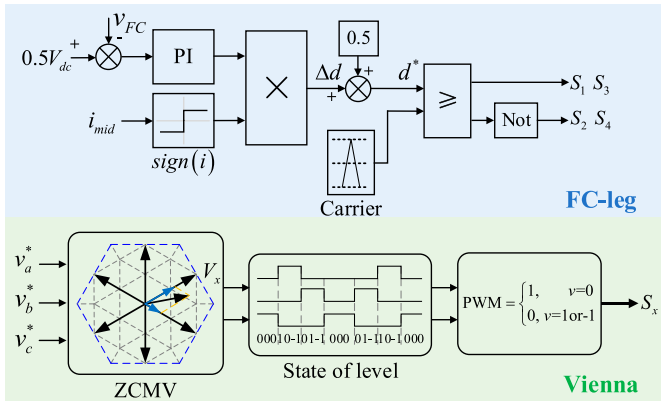


Fig. 7. Control method of FC-Vienna.

with the carrier wave. The PWM for S_2 and S_4 are then opposite to those of S_1 and S_3.

Next, we will discuss the effectiveness of this control method. As shown in Fig. 7, let us assume that at this moment $i_{\text{mid}} > 0$ and $v_{\text{FC}} < 0.5V_{\text{dc}}$. In this case, the Δd is greater than 0. Therefore, the conduction time of S_1 and S_3 increases, leading to a longer charging time for the capacitor and an increase in the v_{FC}. When $v_{\text{FC}} > 0.5V_{\text{dc}}$, the Δd is less than 0. Consequently, the conduction time of S_2 and S_4 increases, resulting in a longer discharge time for the capacitor and a decrease in the v_{FC}. This process stabilizes the capacitor voltage v_{FC} at $0.5V_{\text{dc}}$. The same principle applies when $i_{\text{mid}} < 0$.

IV. Analysis and Compensation of Nonideal Factors

A. The Unidirectional Conductivity of Diodes

The Vienna rectifier has two diodes per phase, and diodes are uncontrolled devices. They conduct when subjected to a positive voltage and turn off when subjected to a negative voltage. Therefore, when current flows from the ac side into a bridge arm ($i > 0$), the ac input voltage for that phase can only be $V_{\text{dc}}/2$ or zero level, not $-V_{\text{dc}}/2$. When the current flows from the bridge arm into the ac side ($i < 0$), the ac input voltage for

Authorized licensed use limited to: Univ of Calif Berkeley. Downloaded on October 27,2026 at 23:27:44 UTC from IEEE Xplore. Restrictions apply.

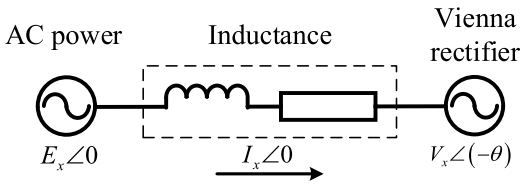


Fig. 8. Equivalent diagram of the circuit of the Vienna rectifier.

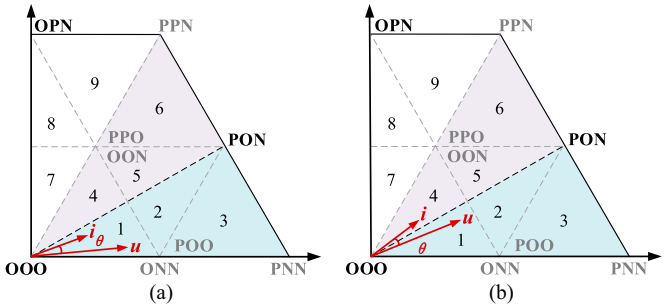


Fig. 9. Composition of vectors. (a) Same sign. (b) Different sign.

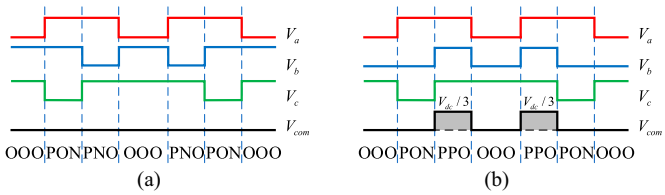


Fig. 10. Waveform of phase voltage and CMV in distortion range. (a) Ideal ZCMV. (b) Actual ZCMV.

that phase can only be $-V_{\rm dc}/2$ or zero level, not $V_{\rm dc}/2$. Consequently, the operating state of the Vienna rectifier is restricted by the unidirectional conductivity of diodes and is determined by the direction of the current.

B. The Current Distortion

When the Vienna rectifier operates in a steady-state, the power factor on the grid side is essentially 1. Therefore, the grid voltage e_x ($x = a, b, c$), is in phase with the current i_x, as shown in Fig. 8. Due to the filtering inductance L on the ac-side, there is inevitably a phase difference between the rectifier's input current i_x and voltage u_x. Because the equivalent resistance R_s of the inductance is much smaller compared to the rectifier's output voltage, it can be neglected. The phase angle θ can be calculated using the following:

$$\theta = \tan^{-1}\left(\frac{2\pi f L I_x}{V_x - R_s I_x}\right) \approx \tan^{-1}(2\pi f L I_x / V_x) \tag{6}$$

where f is the frequency of the modulation wave, I_x is the current of the ac, and V_x is the voltage of the ac.

Because the phase of the current is ahead of the voltage, there will be situations where current and voltage have different symbols. The following is to reveal the principle of current distortion by analyzing the synthesis of vectors in different cases. As shown in Fig. 9.

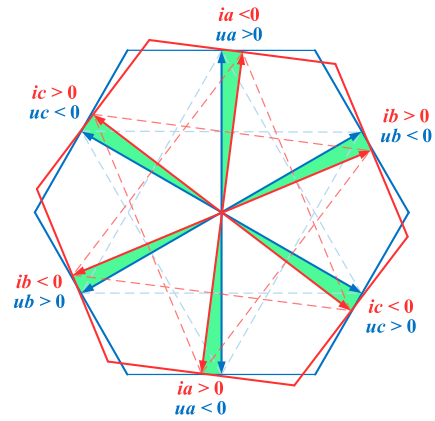


Fig. 11. Range of current distortion.

1) Vector Synthesis of Current and Voltage With the Same Sign: When i_x and u_x have the same sign, as shown in Fig. 9(a). i_x and u_x are both in the blue triangle, at this time $u_a > 0$, $i_a > 0$, $u_b < 0$, $i_b < 0$, $u_c < 0$, and $i_c < 0$. In this case, the voltage of phase a is $V_{\rm dc}/2$ and 0, while the voltage of phases b and c is $-V_{\rm dc}/2$ and 0. If the voltage vector is in Section I, it can be synthesized by [OOO], [POO], [ONN], and [OON]. If the voltage vector is in Section II, it can be synthesized by [ONN], [POO], [PON], and [OON]. If the voltage vector is in Section III, it can be synthesized by [ONN], [POO], [PNN], and [PON]. Voltage vectors can be accurately synthesized.

2) Vector Synthesis of Current and Voltage With the Different Sign: When the current vector i transitions from the blue triangle to the purple triangle while the voltage vector u remains in the blue triangle, i_b changes from negative to positive, while u_b remains negative, as shown in Fig. 9(b). At this moment, $u_a > 0$, $i_a > 0$, $u_b < 0$, $i_b > 0$, $u_c < 0$, $i_c < 0$. In this case, the voltage of phase a can be $V_{\rm dc}/2$ and 0. Due to the constraints of diode unidirectional conductivity, the voltage of phase b can only be $V_{\rm dc}/2$ and 0. The voltage of phase c can be $-V_{\rm dc}/2$ and 0. If the voltage vector is in Section I, it can be synthesized by [OOO], [POO], and [OON]. If the voltage vector is in Section II, it can be synthesized by [POO], [PON], and [OON]. The above two sections can still be accurately synthesized. It is worth noting that if the voltage vector is in Section III, because the voltage of phase b cannot be $-V_{\rm dc}/2$, only [POO] and [PON] can be used, and [PNN] becomes [PPN], so the voltage vector cannot be accurately synthesized, resulting in current distortion. In ZCMV modulation, when $i_b > 0$ and $u_b < 0$, [PNO] becomes [PPO], resulting in a CMV with an amplitude of $V_{\rm dc}/3$. As shown in Fig. 10.

The blue in Fig. 11 is the space vector diagram of the phase voltage, the red is the space vector diagram of the grid voltage (current), and the green is the range of current distortion.

Because the grid voltage phase-locked control is used, the grid voltage vector angle is taken as the reference angle, thus the theoretical distortion range shown in Table II can be obtained.

C. Current Ripple and Delay

As shown in Fig. 12, due to the presence of ripples in the actual ac-side current and quantization errors and delay errors in

Authorized licensed use limited to: Univ of Calif Berkeley. Downloaded on October 27,2026 at 23:27:44 UTC from IEEE Xplore. Restrictions apply.

TABLE II
THEORETICAL INTERVAL OF CURRENT DISTORTION

Phase	Distortion Range
a	$\varphi_a = [90°, 90° + \theta]$ and $[270°, 270° + \theta]$
b	$\varphi_b = [30°, 30° + \theta]$ and $[210°, 210° + \theta]$
c	$\varphi_c = [150°, 150° + \theta]$ and $[330°, 330° + \theta]$

Note: θ is calculated by (6). φ_x is distortion range of phase x.

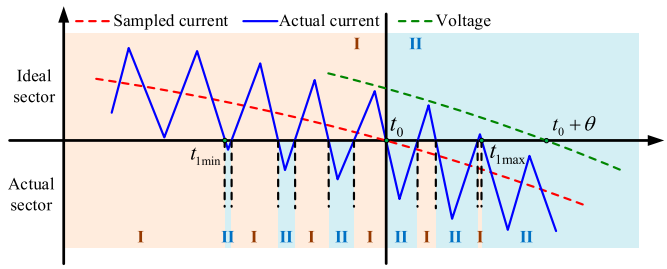


Fig. 12. Sectors are repeatedly identified.

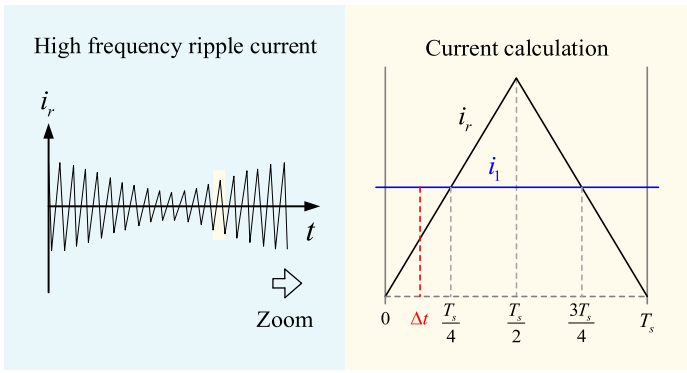


Fig. 13. Reconstruction of current.

current sampling and feedback, there may be instances when the sampled current has the opposite sign compared to the actual current when the current crosses zero. Consequently, the sectors near the zero-crossing of the current will be repeatedly identified.

As shown in Fig. 13, the actual current is reconstructed by adding the sampled low-frequency fundamental current i_1 and the high-frequency ripple current i_r predicted based on the software algorithm. The value of i_r is calculated using the following:

$$i_r = \begin{cases} k\left(\Delta t - \dfrac{T_s}{4}\right) = \dfrac{u_L}{L}\left[(t \bmod T_s) - \dfrac{T_s}{4}\right], 0 \le \Delta t \le \dfrac{T_s}{2} \\ k\left(\dfrac{3T_s}{4} - \Delta t\right) = \dfrac{u_L}{L}\left[\dfrac{3T_s}{4} - (t \bmod T_s)\right], \dfrac{T_s}{2} < \Delta t \le T_s \end{cases} \tag{7}$$

where k is the slope of the ripple, t is time, T_s is the switching period, "mod" represents the modulo operation (e.g., 5 mod 2 = 1), which means the remainder when t is divided by T_s is represented as Δt, u_L is the voltage of the inductance, calculated by (1), and L is the inductance.

TABLE III
COMPENSATION METHOD BASED ON VOLTAGE INJECTION

Range	φ_a	φ_b	φ_c	Other
V_a	0	$U_a^* + 0.5U_b^*$	$U_a^* + 0.5U_c^*$	U_a^*
V_b	$U_b^* + 0.5U_a^*$	0	$U_b^* + 0.5U_c^*$	U_b^*
V_c	$U_c^* + 0.5U_a^*$	$U_c^* + 0.5U_b^*$	0	U_c^*

Note: U_x^* $(x = a, b, c)$ is the set value of the modulation wave for that phase after closed-loop control, V_x is the value of the modulation wave after compensation, and φ_x is calculated from Table II. "Other" indicates range where none of the three phases experience current distortion.

The actual current i is as follows:

$$i = i_1 + i_r. \tag{8}$$

As shown in Fig. 12, taking the example of the influence of current ripple on the range of current distortion when the current transitions from positive to negative, the same reasoning applies when the current transitions from negative to positive. Define the zero crossing of the sampled fundamental current as t_0. The zero crossing of the actual current is denoted as t_1, where the min is $t_{1\min}$, and the max is $t_{1\max}$. The methods for solving $t_{1\min}$ and $t_{1\max}$ are as follows:

$$\begin{cases} t_{1\min} = \min[i = 0] \quad \text{and} \quad i_1(t_{1\min}) > 0 \\ t_{1\max} = \max[i = 0] \quad \text{and} \quad i_1(t_{1\max}) < 0 \end{cases} \tag{9}$$

where $\min[i = 0]$ represents the min value of t for which $i = 0$, and $\max[i = 0]$ represents the max value of t for which $i = 0$. $i_1(t_{1\min}) > 0$ indicates that at the moment $t_{1\min}$, the value of i_1 is greater than 0. The condition $i_1(t_{1\max}) > 0$ indicates that at the moment $t_{1\max}$, the value of i_1 is less than 0. This is to restrict the current from transitioning from positive to negative. Therefore, the range for considering current distortion after accounting for current ripple should be as follows:

$$[t_{1\min}, \max[t_{1\max}, t_0 + \theta]]. \tag{10}$$

Communication and switching delays in practical systems prevent the pulses of ZCMV modulation from aligning perfectly, resulting in the presence of spikes in CMV.

D. ZCMV Modulation With Compensation for Nonideal Factors

Based on the analysis above, because the current and voltage with the different sign in the current distortion range, there are many spikes in the CMV in normal ZCMV modulation. Therefore, when phase x enters the distortion zone, set its voltage value to 0, then the switch is always on, and the phase x voltage is clamped to 0, and there is no $\pm V_{dc}/2$ due to the current direction, thus suppressing the distortion. On this basis, we propose a new compensation method based on voltage injection. It can completely eliminate CMV in the distortion range. Its modulation waveforms are shown in Table III.

Therefore, within the range of current distortion, the CMV based on the voltage injection compensation modulation is as follows:

$$V_{com} = \frac{1}{3}(V_a + V_b + V_c) = \frac{1}{3}(U_a^* + U_b^* + U_c^*) = 0. \tag{11}$$

There are ripples in the actual current, and as analyzed in Section IV-C, we should consider the impact of current ripple to

Authorized licensed use limited to: Univ of Calif Berkeley. Downloaded on October 27,2026 at 23:27:44 UTC from IEEE Xplore. Restrictions apply.

TABLE IV
ZCMV WITH NONIDEAL FACTOR COMPENSATION (FC-ZCMV-C)

Range	φ'_a	φ'_b	φ'_c	Other
V'_a	0	$U^*_a+0.5U^*_b$	$U^*_a+0.5U^*_c$	U^*_a
V'_b	$U^*_b+0.5U^*_a$	0	$U^*_b+0.5U^*_c$	U^*_b
V'_c	$U^*_c+0.5U^*_a$	$U^*_c+0.5U^*_b$	0	U^*_c

Note: V'_x is the value of the modulation wave with FC-ZCMV-C.

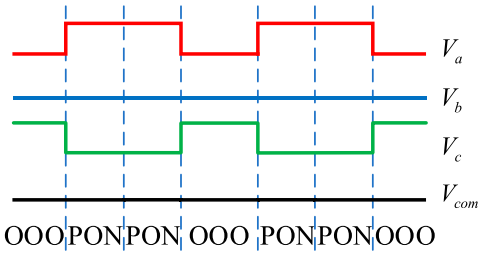


Fig. 14. Waveform of phase voltage and CMV in distortion range with FC-ZCMV-C.

correct the distortion range. Diodes and switches are not ideal devices; they have delays in turning on and off. Additionally, there is a communication delay between the control signal and the voltage change after the final switch action. This makes the zero crossing of the current more complex. Therefore, we also need to consider the impact of delays to further correct the distortion range. The distortion range for phase a of the ZCMV modulation that takes various nonideal factors into account is as shown in (12), and its modulation waveforms are listed in Table IV. This method is called: ZCMV modulation with nonideal factor compensation of the FC-Vienna rectifier (FC-ZCMV-C)

$$\varphi'_a = \begin{matrix}[90^\circ-\alpha_1+\Delta\varphi_1, 90^\circ+\theta+\alpha_2+\Delta\varphi_2] \quad \text{and} \\ [270^\circ-\alpha_3+\Delta\varphi_3, 270^\circ+\theta+\alpha_4+\Delta\varphi_4]\end{matrix} \tag{12}$$

where θ is the phase angle of current leading voltage, calculated from (6). α represents the influence of current ripple on the current distortion interval, calculated from (10). $\Delta\varphi$ represents the impact of switch and communication delays, obtained through experimental observation and debugging. The calculation of φ'_b and φ'_c follows the same principle.

Compare Fig. 10, when in the range of b-phase current distortion. The voltage waveform of FC-ZCMV-C is shown in Fig. 14.

Fig. 15 shows the synthetic error without and with compensation. The phase difference leads to the wrong use of the vector, which reduces the quality of the electrical energy and causes the spikes in CMV in the actual ZCMV. The synthesis error of the green vector of FC-ZCMV-C is less than that of the uncompensated blue vector, thereby mitigating the degradation of power quality resulting from vector misapplication. Additionally, the CMV of the green vector is maintained at zero. The same is true for other distortion ranges.

V. SIMULATION

The simulation models of Vienna and FC-Vienna were constructed in Matlab/Simulink. Four modulation methods, namely SVPWM, ZCMV, ZCMV of FC-Vienna (FC-ZCMV), and

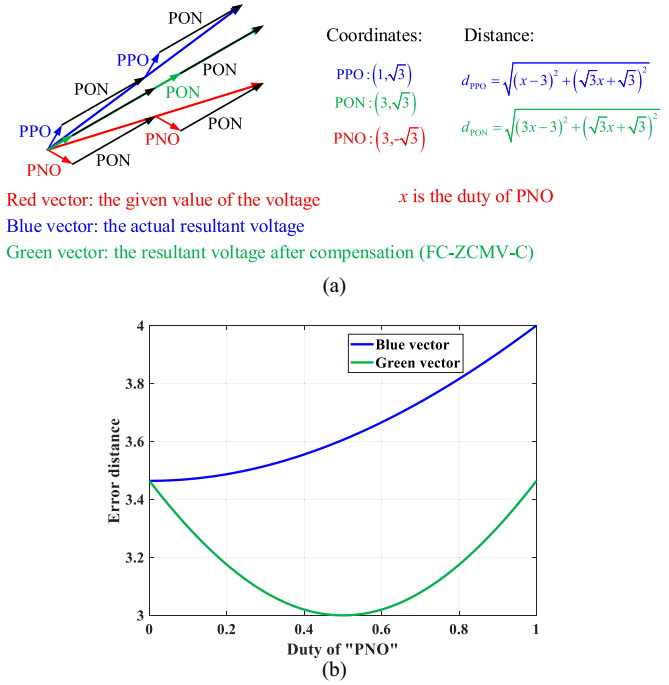


Fig. 15. Voltage synthesis in the range of b-phase current distortion. (a) Principle of synthesis. (b) Comparison of error distances.

TABLE V
PARAMETERS FOR SIMULATION AND EXPERIMENTATION

Symbol	Parameter	Value
e	RMS of the grid voltage	40 V
V^*_{dc}	Dc voltage	200 V
f_s	Switching frequency	20 kHz
f	Modulated wave frequency	50 Hz
C	Voltage regulator capacitor	56 uF
C_F	Flying-capacitor	56 uF
L	Filter inductor	1 mH
R	Lord	100 Ω

FC-ZCMV-C, were verified. Simulation parameters are provided in Table V.

The time domain waveforms of CMV for the four modulation strategies are shown in Fig. 16. The CMV for SVPWM is a step waveform with an amplitude of 66.7 V. For ZCMV and FC-ZCMV, the CMV is mostly zero, but there are many spikes in the range of current distortion, with a time scale of 1 us. This can result in EMI in the MHz frequency range. These two modulation strategies have identical PWM signals, and the difference lies in the suppression of the NPV fluctuation by the FC-leg, which has less impact on the CMV spectrum. Therefore, the CMV analysis focuses only on FC-ZCMV. FC-ZCMV-C eliminates all spikes, and the ripple amplitude is only 0.5 V, significantly reducing CM EMI.

Fig. 17 shows the frequency spectrum of CMV for the three modulation strategies. It can be observed that compared to SVPWM, ZCMV reduces EMI by about 30–40 dB in the 10–400 kHz and by approximately 10 dB in the 400 kHz–5 MHz. In comparison to ZCMV, FC-ZCMV-C reduces EMI by about

Authorized licensed use limited to: Univ of Calif Berkeley. Downloaded on October 27,2026 at 23:27:44 UTC from IEEE Xplore. Restrictions apply.

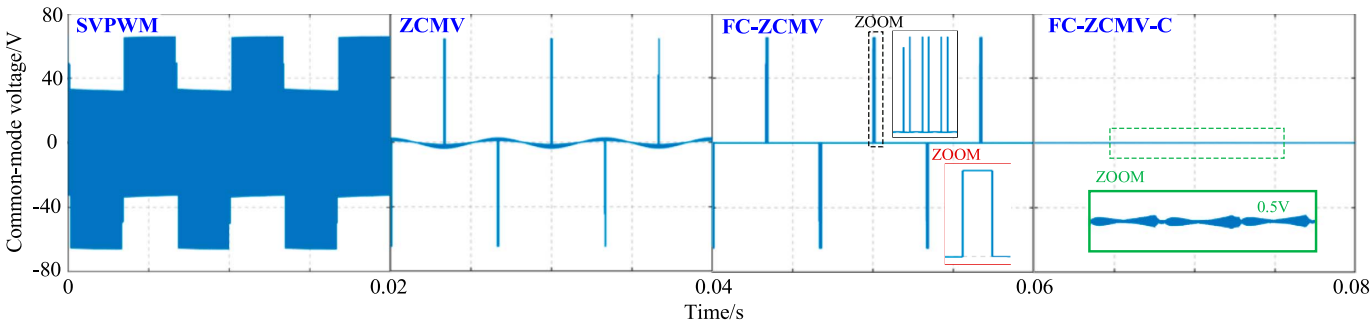


Fig. 16. Time domain waveform of CMV (Simulation).

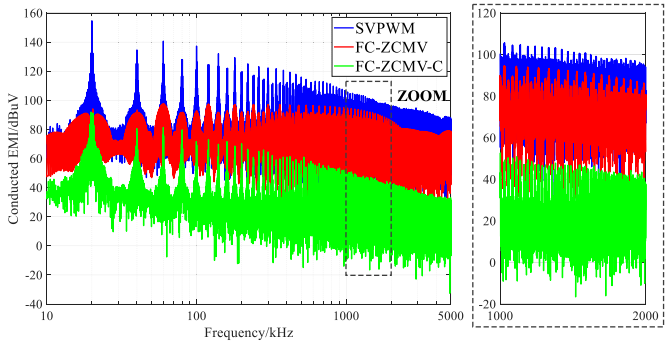


Fig. 17. Spectrum of CMV (Simulation).

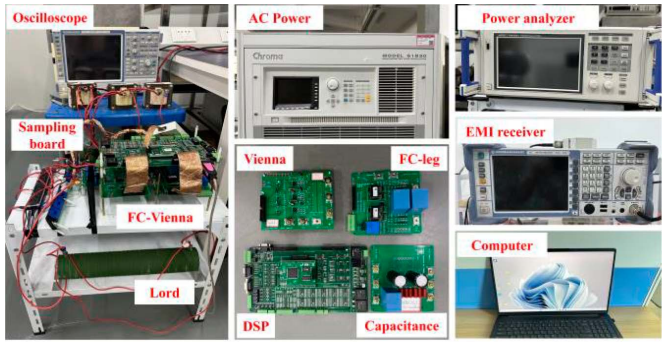


Fig. 18. Experimental platform.

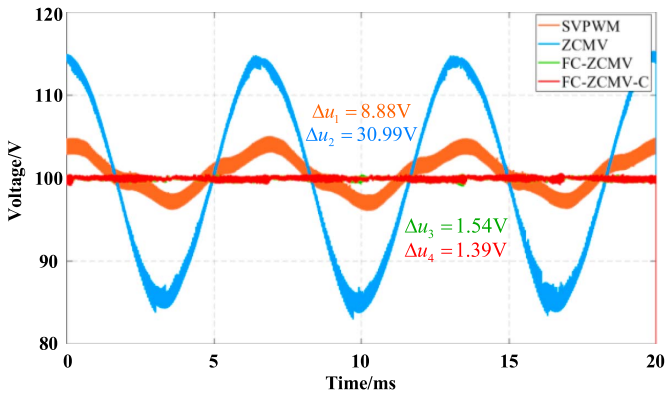


Fig. 19. NPV of the four modulation strategies.

30–40 dB in the 400 kHz–5 MHz, which is caused by spikes in current distortion. In summary, FC-ZCMV-C can reduce EMI by 40–50 dB in the 10 kHz–5 MHz compared to SVPWM.

VI. Experiment

The experimental platform, as shown in Fig. 18, was built in the laboratory. The three-phase ac power supply (Chroma 61830) supplied power to the rectifier and could measure the power factor. The whole system was controlled by the computer and the load was resistance. The Vienna rectifier was composed of the DSP (TMS320F28377D), Vienna, and capacitors, as shown in the figure. The FC-Vienna rectifier consisted of the DSP, Vienna, and the FC-leg. Efficiency was tested using a power analyzer (HIOKI PW6001). Experimental parameters can be found in Table V.

The NPV of the four modulation strategies is shown in Fig. 19. The amplitude of the NPV fluctuation of SVPWM is 8.88 V. Because ZCMV uses only the zero CMV vector, the NPV fluctuation increases to 30.99 V. With the addition of the FC-leg decoupled from the main circuit, the NPV fluctuations are reduced to 1.54 and 1.39 V. Compared with ZCMV, the NPV fluctuation of FC-ZCMV-C is reduced by 95.51%. Compared with SVPWM, the NPV fluctuation of FC-ZCMV-C is reduced by 84.35%.

The time domain waveforms of three-phase currents and CMV for the four modulation strategies are shown in Fig. 20. The CMV for SVPWM is a step waveform with an amplitude of $V_{dc}/3$ (about 67 V). ZCMV reduces the amplitude of CMV but exhibits a low-frequency component due to significant NPV fluctuation (triple frequency fluctuations in CMV are shown in Table VI). FC-ZCMV further suppresses the low-frequency CMV fluctuations by suppressing the NPV fluctuation. However, there are many spikes in the range of current distortion. FC-ZCMV-C suppresses these spikes through compensation, reducing the amplitude of CMV. The experimental results closely match the simulation results. However, due to the experimental conditions not being entirely ideal, the suppression effect on CMV spikes is slightly inferior to that of the simulation.

The spectrum of CMV with three modulation strategies is shown in Fig. 21. It can be seen that compared to SVPWM, FC-ZCMV reduces EMI by about 20 dB at switching frequency doubling. The time scale of CMV spikes caused by current distortion is μs level (as shown in Fig. 16), so there are still spikes at MHz of the spectrum of FC-ZCMV. FC-ZCMV-C reduces the EMI of 5–10 dB at MHz through the suppression method of spikes compensation. In summary, in the frequency band of 10 kHz to several MHz, compared with SVPWM, FC-ZCMV-C can reduce the conducted EMI by 20 dB. Translation: In simulation, FC-ZCMV-C can completely eliminate the spikes of CMV

Authorized licensed use limited to: Univ of Calif Berkeley. Downloaded on October 27,2026 at 23:27:44 UTC from IEEE Xplore. Restrictions apply.

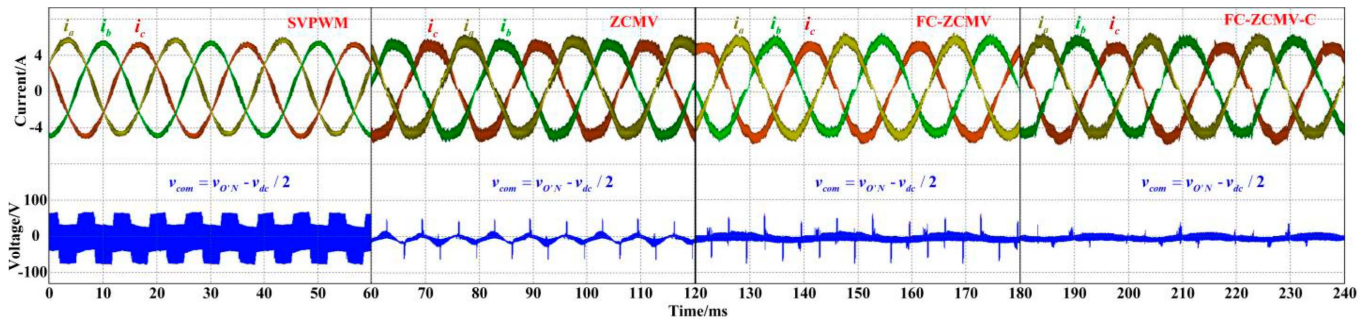


Fig. 20. Current and CMV for the four modulation strategies.

TABLE VI
PERFORMANCE PARAMETERS

Performance	Current THD	Amplitude (150 Hz in CMV)	Power Factor	Efficiency
SVPWM	5.44%	12.63 V	0.998	96.52%
ZCMV	9.29%	10.22 V	0.997	96.54%
FC-ZCMV	9.20%	0.51 V	0.997	96.29%
FC-ZCMV-C	9.13%	0.60 V	0.997	96.34%

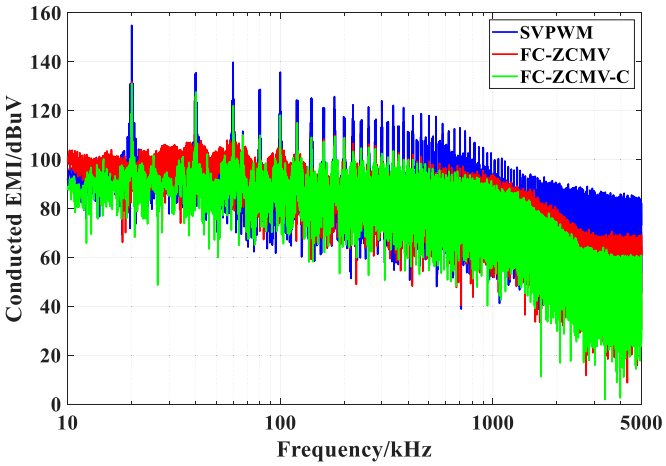


Fig. 21. Spectrum of CMV.

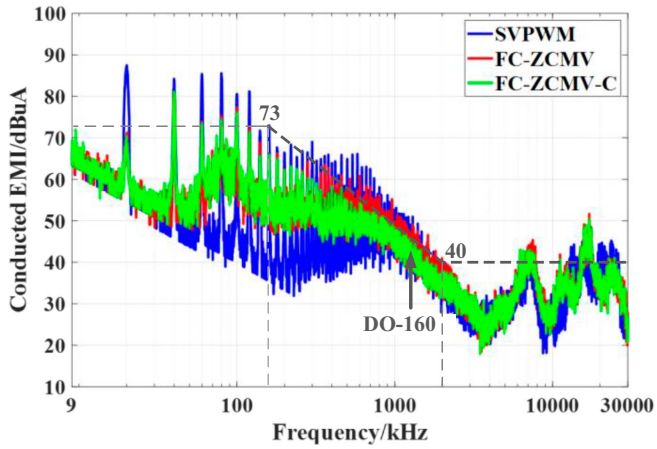


Fig. 22. Spectrum of common mode current.

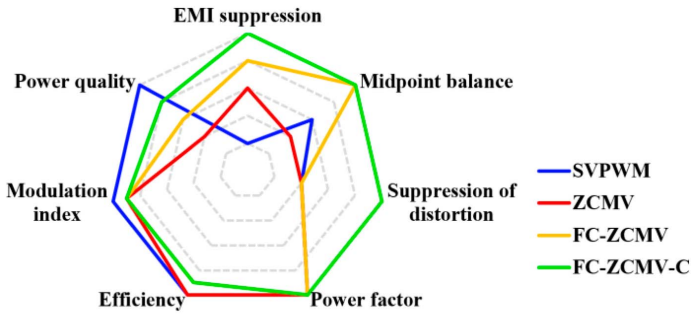


Fig. 23. Comparison of performance.

in the current distortion range, which proves the correctness of the principle. However, due to the fact that the parameters in the experiment are not completely ideal, the suppression capability of CMV is slightly lower than in the simulation. Nevertheless, FC-ZCMV-C still exhibits good suppression effects on CMV.

Fig. 22 is the result of the CM current measured by the EMI receiver. It can be seen that compared with FC-ZCMV, FC-ZCMV-C reduces the EMI of 5–10 dB at 300 kHz–2 MHz through the suppression method of spikes compensation. Compared to SVPWM, FC-ZCMV-C reduces CM interference by 5–15 dB.

Table VI provides additional performance parameters for the four modulation strategies.

Fig. 23 presents a comprehensive comparison of them. The comparison of EMI suppression and midpoint balancing are sourced from Figs. 19 and 22. The comparison of modulation degree comes from the analysis in Section II-B. ZCMV modulation. All other performance comparisons are sourced from Table VI. A higher index indicates better performance, including better CMV suppression, smaller NPV fluctuation, less current distortion, higher power factor, higher efficiency, and higher power quality. Therefore, the larger the area, the better the overall performance. It can be observed that FC-ZCMV-C effectively suppresses CMV without compromising the power factor, reduces NPV fluctuation, and suppresses current distortion. The disadvantage is that it slightly reduces efficiency and modulation index.

Authorized licensed use limited to: Univ of Calif Berkeley. Downloaded on October 27,2026 at 23:27:44 UTC from IEEE Xplore. Restrictions apply.

VII. Conclusion

This article begins by analyzing CMV in the Vienna rectifier. We achieve CMV suppression by using only medium vectors and zero vector. Next, it derives the reasons for current distortion in the Vienna rectifier and analyzes the impact of nonideal factors such as current ripple and control delay. Finally, a new ZCMV modulation strategy which considering compensation for various nonideal factors was proposed. Simulation results have verified the theoretical correctness. The experimental results demonstrate that FC-ZCMV-C can significantly reduce the amplitude of CMV without affecting power factor, suppress spikes caused by various nonideal factors, and reduce conducted EMI by 10–20 dB. At the same time, it can significantly reduce the fluctuation of NPV, and it can also suppress current distortion. The FC-leg adds very little to the cost and does not increase the size of the system. The disadvantage was that the THD of the current was increased and the modulation index was reduced. The method was relatively simple, and the control of FC-leg was decoupled from the main circuit, so it was suitable for Vienna rectifier on various occasions.

References

[1] J. W. Kolar, U. Drofenik, and F. C. Zach, "VIENNA rectifier II-a novel single-stage high-frequency isolated three-phase PWM rectifier system," *IEEE Trans. Ind. Electron.*, vol. 46, no. 4, pp. 674–691, Aug. 1999.

[2] M. Zhang, Y. Yuan, X. Sun, Y. Zhang, and X. Li, "Harmonic resonance suppression strategy of the front-end Vienna rectifier in EV charging piles," *IEEE Trans. Power Electron.*, vol. 38, no. 1, pp. 1036–1053, Jan. 2023.

[3] J.-S. Lee and K.-B. Lee, "A novel carrier-based PWM method for Vienna rectifier with a variable power factor," *IEEE Trans. Ind. Electron.*, vol. 63, no. 1, pp. 3–12, Jan. 2016.

[4] A. Rajaei, M. Mohamadian, and A. Yazdian Varjani, "Vienna-rectifier-based direct torque control of PMSG for wind energy application," *IEEE Trans. Ind. Electron.*, vol. 60, no. 7, pp. 2919–2929, Jul. 2013.

[5] L. Fan et al., "Analysis and utilization of common-mode voltage in inverters for power supply," *Trans. Power Electron.*, vol. 38, no. 7, pp. 8811–8824, Jul. 2023.

[6] F. Krismer, S. Schroth, H. Ertl, K. S. Kostov, H.-P. Nee, and J. W. Kolar, "Analysis and practical relevance of CM/DM EMI noise separator characteristics," *IEEE Trans. Power Electron.*, vol. 32, no. 4, pp. 3112–3127, Apr. 2017.

[7] D. Han, C. T. Morris, and B. Sarlioglu, "Common-mode voltage cancellation in PWM motor drives with balanced inverter topology," *IEEE Trans. Ind. Electron.*, vol. 64, no. 4, pp. 2683–2688, Apr. 2017.

[8] X. Li, Y. Sun, L. Jiang, H. Wang, Y. Liu, and M. Su, "Common-mode circuit analysis of current-source photovoltaic inverter for leakage current and EMI," *IEEE Trans. Power Electron.*, vol. 38, no. 6, pp. 7156–7165, Jun. 2023.

[9] C. Labarre and F. Costa, "Circuit analysis of an EMI filter for the prediction of its magnetic near-field emissions," *IEEE Trans. Electromagn. Compat.*, vol. 54, no. 2, pp. 290–298, Apr. 2012.

[10] H. Li, Y. Ding, C. Zhang, Z. Yang, Z. Yang, and B. Zhang, "A compact EMI filter design by reducing the common-mode inductance with chaotic PWM technique," *IEEE Trans. Power Electron.*, vol. 37, no. 1, pp. 473–484, Jan. 2022.

[11] Y. Zhou et al., "A new integrated active EMI filter topology with both CM noise and DM noise attenuation," *IEEE Trans. Power Electron.*, vol. 37, no. 5, pp. 5466–5478, May 2022.

[12] L. Guo, N. Jin, C. Gan, and K. Luo, "Hybrid voltage vector preselection-based model predictive control for two-level voltage source inverters to reduce the common-mode voltage," *IEEE Trans. Ind. Electron.*, vol. 67, no. 6, pp. 4680–4691, Jun. 2020.

[13] E. Un and A. M. Hava, "A near-state PWM method with reduced switching losses and reduced common-mode voltage for three-phase voltage source inverters," *IEEE Trans. Ind. Appl.*, vol. 45, no. 2, pp. 782–793, Mar./Apr. 2009.

[14] X. Xu et al., "Common-mode voltage reduction for back-to-back two-level converters based on zero-sequence voltage injection," *IEEE Trans. Ind. Electron.*, vol. 70, no. 12, pp. 11971–11982, Dec. 2023.

[15] J. Chen, D. Jiang, W. Sun, and X. Pei, "Common-mode voltage reduction scheme for MMC With low switching frequency in AC–DC power conversion system," *IEEE Trans. Ind. Informat.*, vol. 18, no. 1, pp. 278–287, Jan. 2022.

[16] X. Xu, Z. Zheng, K. Wang, B. Yang, and Y. Li, "A carrier-based common-mode voltage elimination method for back-to-back three-level NPC converters," *IEEE Trans. Power Electron.*, vol. 37, no. 3, pp. 3040–3052, Mar. 2022.

[17] A. Hota and V. Agarwal, "Novel three-phase H10 inverter topology with zero or constant common-mode voltage for three-phase induction motor drive applications," *IEEE Trans. Ind. Electron.*, vol. 69, no. 7, pp. 7522–7525, Jul. 2022.

[18] Z. Shen, D. Jiang, Z. Liu, D. Ye, and J. Li, "Common-mode voltage elimination for dual two-level inverter-fed asymmetrical six-phase PMSM," *IEEE Trans. Power Electron.*, vol. 35, no. 4, pp. 3828–3840, Apr. 2020.

[19] S. Xia, X. Wu, J. Zheng, X. Li, and K. Wang, "A virtual space vector PWM with active neutral point voltage control and common mode voltage suppression for three-level NPC converters," *IEEE Trans. Ind. Electron.*, vol. 68, no. 12, pp. 11761–11771, Dec. 2021.

[20] M. Perotti and F. Fiori, "A closed loop delay compensation technique to mitigate the common mode conducted emissions of bipolar PWM switched circuits," *IEEE Trans. Power Electron.*, vol. 36, no. 5, pp. 5450–5459, May 2021.

[21] B. Lee, Z. Q. Zhu, and D. Wu, "On-load voltage distortion compensation method using disturbance observer for SPM machines with closed slot," *Chin. J. Elect. Eng.*, vol. 1, no. 1, pp. 58–69, Dec. 2015.

[22] Z. Miao, H. Tong, X. Jin, W. Yao, Z. Lu, and Z. Ma, "DQ-frame zero-crossing effect modeling and current distortion compensation method for Vienna rectifier," *IEEE Trans. Power Electron.*, vol. 35, no. 7, pp. 7612–7623, Jul. 2020.

[23] X. Xing, X. Li, C. Qin, Z. Liu, and C. Zhang, "Two-layer pulsewidth modulation strategy for common-mode voltage and current harmonic distortion reduction in Vienna rectifier," *IEEE Trans. Ind. Electron.*, vol. 67, no. 9, pp. 7470–7483, Sep. 2020.

[24] H. Liu, X. Zhao, D. Jiang, M. Zhou, and S. Zhang, "Zero common-mode voltage modulation in novel flying-capacitive VIENNA rectifier," in *Proc. 11th Int. Conf. Power Electron. ECCE Asia (ICPE—ECCE Asia)*, Jeju Island, South Korea, 2023, pp. 2649–2654.

[25] W. Li, Y. Wang, J. Hu, H. Yang, C. Li, and X. He, "Common-mode current suppression of transformerless nested five-level converter with zero common-mode vectors," *IEEE Trans. Power Electron.*, vol. 34, no. 5, pp. 4249–4258, May 2019.

[26] M. Lak, B.-R. Chuang, and T.-L. Lee, "A common-mode voltage elimination method with active neutral point voltage balancing control for three-level T-type inverter," *IEEE Trans. Ind. Appl.*, vol. 58, no. 6, pp. 7499–7514, Nov./Dec. 2022.

[27] W. Li, X. Zhang, and D. Xu, "Integrated modulation of dual-parallel NPC inverters with eliminated CMV," *IEEE Trans. Ind. Electron.*, vol. 69, no. 8, pp. 8113–8122, Aug. 2022.

[28] D. Han, S. Li, W. Choi, and B. Sarlioglu, "Design, implementation, and evaluation of a GaN-based four-leg inverter with minimal common mode voltage generation," in *Proc. IEEE Energy Convers. Congr. Expo. (ECCE)*, Cincinnati, OH, USA, 2017, pp. 5383–5388.



Hui Liu (Student Member, IEEE) received the B.S. degree in electrical engineering from Hefei University of Technology, Hefei, China, in 2021. He is currently working toward the Ph.D. degree in electrical engineering with Huazhong University of Science and Technology, Wuhan, China.

His research interests include multilevel converters and electromagnetic interference of power electronics.

Authorized licensed use limited to: Univ of Calif Berkeley. Downloaded on October 27,2026 at 23:27:44 UTC from IEEE Xplore. Restrictions apply.



Dong Jiang (Senior Member, IEEE) received the B.S. and M.S. degrees in electrical engineering from Tsinghua University, Beijing, China, in 2005 and 2007, respectively, and the Ph.D. degree in power electronics and motor drives from the University of Tennessee, Knoxville, TN, USA, in 2011.

From January 2012 to July 2015, he was a Senior Research Scientist/Engineer with the United Technologies Research Center, East Hartford, CT, USA. Since, July 2015, he has been a Professor with Huazhong University of Science and Technology, Wuhan, China. His research interests include power electronics and motor drives. He has published more than 100 IEEE journal and conference papers and more than 40 granted patents in this area.

Dr. Jiang was an Associate Editor for IEEE TRANSACTIONS ON INDUSTRY APPLICATIONS. He was the recipient of several best paper awards in IEEE conferences.



Shuyu Zhang received the B.Eng. degree in electrical engineering from Huazhong University of Science and Technology, Wuhan, China, in 2023. She is currently working toward the master's degree in electrical engineering with Stanford University, Stanford, CA, USA.

Her research interests include multilevel converters, electromagnetic interference elimination, and voltage regulator modules based on switched-capacitor topologies.



Xuan Zhao (Student Member, IEEE) received the B.S. and M.S. degrees in 2017 and 2020, respectively, from Huazhong University of Science and Technology, Wuhan, China, where he is currently working toward the Ph.D. degree, all in electrical engineering.

His research interests include multilevel converters, ac motor drive, and electromagnetic interference of power electronics system.



Zicheng Liu (Member, IEEE) received the B.S. degree in hydropower engineering from Huazhong University of Science and Technology (HUST), Wuhan, China, in 2011, and the Ph.D. degree in electrical engineering from Tsinghua University, Beijing, China, in 2016.

From October 2014 to March 2015, he was a Visiting Student with Purdue University, West Lafayette, IN, USA. From June 2016 to September 2018, he was a Postdoctoral Researcher with Beijing Jiaotong University, Beijing, China. He is currently an Associate Professor with HUST. His research interests include multiphase motor control systems and transportation electrification.

Dr. Liu was the recipient of two prize paper awards in IEEE conferences and the second-place prize paper award of IEEE JOURNAL OF EMERGING AND SELECTED TOPICS IN POWER ELECTRONICS. He was the Vice Chair of IEEE Power Electronics Society Wuhan Chapter.

Authorized licensed use limited to: Univ of Calif Berkeley. Downloaded on October 27,2026 at 23:27:44 UTC from IEEE Xplore. Restrictions apply.